Current Biology

Swimming motions evoke Piezo1-dependent Ca²⁺ events in vascular endothelial cells of larval zebrafish

Highlights

- Body motions in larval zebrafish evoke Ca²⁺ signals in vascular endothelial cells
- These Ca²⁺ signals do not require heartbeat, blood flow, or neural activity
- Mechanical forces are necessary and sufficient for endothelial Ca²⁺ transients
- Endothelial Ca²⁺ transients require the mechanosensitive ion channel Piezo1

Authors

Bill Z. Jia, Xin Tang, Marlies P. Rossmann, Leonard I. Zon, Florian Engert, Adam E. Cohen

Correspondence

cohen@chemistry.harvard.edu

In brief

Jia et al. show that, in larval zebrafish, Ca²⁺ signals in vascular endothelial cells are triggered by body motion, not blood flow. This mechanosensitive signal requires the expression of Piezo1.

Current Biology



Report

Swimming motions evoke Piezo1-dependent Ca²⁺ events in vascular endothelial cells of larval zebrafish

Bill Z. Jia, 1,5,8 Xin Tang, 1,6,8 Marlies P. Rossmann, 2,3,7 Leonard I. Zon, 2,3 Florian Engert, 4 and Adam E. Cohen 1,9,*

SUMMARY

Calcium signaling in the vascular endothelium regulates vascular growth, 1,2 immune responses, 3 and tone. 4 Endothelial cells (ECs) are mechanosensitive, 5-7 and flow-driven shear stress is widely assumed to be the main trigger for EC Ca²⁺ responses *in vivo*.^{8–10} Vascular ECs experience a range of distinct mechanical forces in vivo. 1,2,6,7 These include shear stress from blood flow, radial stretch from blood pressure, circumferential stretch from smooth-muscle-mediated vasodilation, and, in some parts of the animal, axial stretch from skeletal-muscle-mediated body motion^{6,11} In principle, these different modes of stimulation could activate distinct signaling pathways and cellular responses. 12-14 Mechanical perturbation experiments on cultured cells or explants typically impose stresses that differ in magnitude and direction from the forces encountered in vivo, 5,15,16 and thus they cannot readily be used to assign biochemical responses to specific sources of mechanical stress in vivo. Here, we show that, in larval zebrafish, the dominant trigger for vascular endothelial Ca²⁺ events comes from body motion, not heartbeat-driven blood flow. Through a series of pharmacological and mechanical perturbations, we showed that body motion is necessary and sufficient to induce endothelial Ca²⁺ events, while neither neural activity nor blood circulation is necessary or sufficient. CRISPR-Cas9 knockout and temporally restricted photomorpholino knockdown identified Piezo1 as necessary for the rapid, mechanically evoked EC Ca²⁺ events. 10,17 Our results demonstrate that swimming-induced tissue motion is an important driver of endothelial Ca²⁺ dynamics in larval zebrafish.

RESULTS

Body motion of larval zebrafish triggers EC Ca²⁺ events in vivo

We performed whole-body fluorescence imaging of larval zebrafish expressing the Ca²⁺ indicator jGCaMP6s¹⁸ under the control of the endothelial cell (EC)-specific *kdrl* promoter *Tg(kdrl: Gal4: UAS: GCaMP6s)* (Figure 1A). We exploited the aversive visualmotor reflex of zebrafish larvae to violet light¹⁹ to trigger a reproducible and naturalistic series of escape twitches (Figures 1A and 1B).

Resting fish showed few spontaneous EC Ca²⁺ events. Escape twitches were followed by a Ca²⁺ increase in blood vessels distributed throughout the tail, including the intersegmental vessels (ISVs), dorsal aorta (DA), and dorsal longitudinal anastomotic vessels (DLAVs; Figure 1B; Video S1). Qualitatively similar

motion-triggered EC Ca²⁺ events occurred in fish at 2, 5, and 7 days post fertilization (dpf) (Figure 1B). We focused on intersegmental ECs to sample, within each field of view, multiple vessels that had similar geometries and experienced similar mechanical forces.

To control for motion artifacts, we repeated these experiments in 5 dpf larvae expressing an eGFP marker in the ECs, Tg(kdrl: eGFP). These fish did not show sustained motion-induced fluorescence transients (Figure 1C). We quantified the fluorescence response amplitudes ($\Delta F/F$ 10 s after motion, ($\Delta F/F$)_{10s}) and found that the response in the GFP-expressing fish was much smaller than that in the GCaMP-expressing fish (eGFP: ($\Delta F/F$)_{10s} = -0.007 (-0.044-0.015), (median [interquartile range, IQR]), n = 5 fish; jGCaMP6s: ($\Delta F/F$)_{10s} = 0.54 (0.16–0.99), n = 8 fish; Figures 1C–1E, statistical tests in figure caption).

¹Department of Chemistry and Chemical Biology, Harvard University, Cambridge, MA 02138, USA

²Department of Stem Cell and Regenerative Biology, Harvard University, Cambridge, MA 02138, USA

³Stem Cell Program and Division of Hematology/Oncology, Boston Children's Hospital and Dana Farber Cancer Institute, Howard Hughes Medical Institute, Harvard Stem Cell Institute, Harvard Medical School, Boston, MA 02115, USA

⁴Department of Molecular and Cellular Biology, Harvard University, Cambridge, MA 02138, USA

⁵Present address: Department of Physiology, University of California, San Francisco, San Francisco, CA 94158, USA

⁶Present address: Department of Mechanical & Aerospace Engineering, University of Florida, Gainesville, FL 32611, USA

Present address: Department of Biomedical Genetics, University of Rochester School of Medicine and Dentistry, Rochester, NY 14642, USA

⁸These authors contributed equally

⁹Lead contact

^{*}Correspondence: cohen@chemistry.harvard.edu https://doi.org/10.1016/j.cub.2025.10.053

CellPress

Current Biology Report

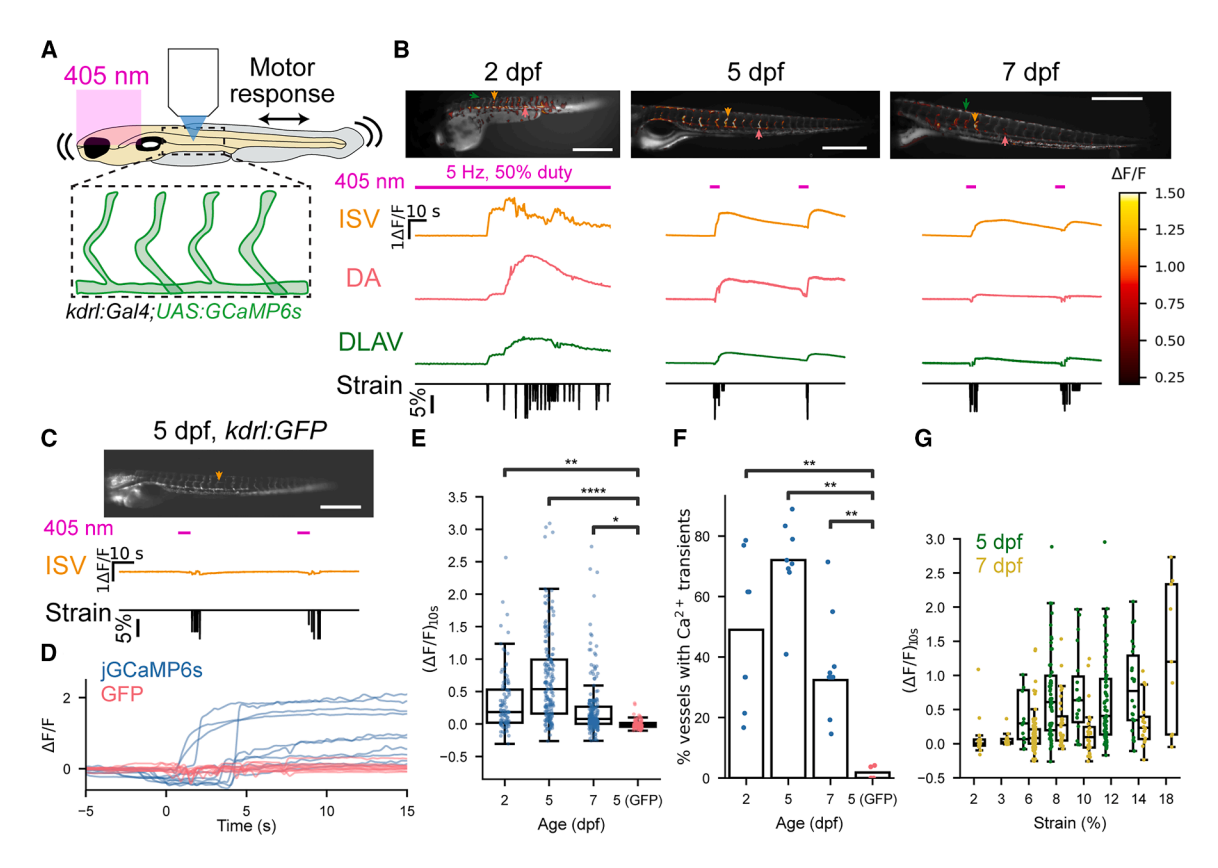


Figure 1. Vascular EC calcium events arise during swim motions in larval zebrafish

- (A) Experimental setup. Violet light on the eyes evoked escape attempts; Ca²⁺ responses were monitored in vascular ECs.
- (B) Vascular ECs of larval zebrafish show Ca^{2+} events at 2, 5, and 7 dpf. Top: composite images of basal fluorescence (grayscale) and $\Delta F/F$ 10 s after motion onset (heatmap). Bottom: 405 nm stimulus, $\Delta F/F$ time traces of Ca^{2+} dynamics on intersegmental vessel (ISV), dorsal aorta (DA), and dorsal longitudinal anastomotic vessel (DLAV), 20,21 and body strain (STAR Methods).
- (C) Images and traces for Tg(kdrl:GFP) fish as in (B).
- (D) Comparison of ΔF/F on swim motion in 10 representative vessels expressing jGCaMP6s (blue) or GFP (red).
- (E) Quantification of $\Delta F/F$ 10 s after motion onset. Each point is a single vessel measured at a single twitch.
- (F) Fraction of measured vessels where Ca²⁺ elevation exceeds 3 standard deviations of GFP ΔF/F, 10 s after motion. Each point is an individual fish.
- (G) Fluorescence response vs. body strain at 5 and 7 dpf. Each point is a single vessel during a single twitch.
- (D–G) Tg(kdrl:Gal4;UAS:GCaMP6s) 2 dpf, 100 vessel-twitch events measured over n = 8 fish; 5 dpf, 179 vessel-twitch events measured over n = 8 fish; 7 dpf, 216 vessel-twitch events measured over n = 9 fish; Tg(kdrl:GFP) 5 dpf, 110 vessel-twitch events measured over n = 5 fish.

Statistical tests: (E) mixed-effects linear model considering individual fish and experimental condition. 2 dpf vs. GFP, p = 3.9e-3, z = -2.9; 5 dpf vs. GFP, p = 7.8e-10, z = -6.2; 7 dpf vs. GFP, p = 3.9e-3, z = -2.2. (F) Mann-Whitney-Wilcoxon test. 2 dpf vs. GFP, p = 3.1e-3, U = 45; 5 dpf vs. GFP, p = 4.1e-3, U = 40; 7 dpf vs. GFP, p = 4.0e-3, U = 40. (H) Spearman correlation. 5 dpf, r = -0.21, p = 0.43; 7 dpf, r = 0.64, p = 1.8e-3. Scale bars, 500 μ m. Additional supporting data in Figure S1.

See also Video S1.

Motion-coupled Ca²⁺ events were also observed at 2 dpf ((Δ F/F)_{10s} = 0.54 (0.02–0.53), n = 8 fish) and at 7 dpf ((Δ F/F)_{10s} = 0.07 (0.002–0.27), n = 9 fish). The percentage of ISVs showing Ca²⁺ transients was 59%, 78%, and 41% at 2, 5, and 7 dpf, respectively, compared with 4% of kdrl:GFP vessels analyzed using the same Δ F/F threshold (Figure 1F). In 5 dpf fish, the median onset time of Ca²⁺ transients was 0.44 (0.04–1.94) s after the start of an escape twitch. The transients decayed with a median time constant of 22.5 (19.8–26.6) s (n = 31 events in two fish; Figure S1).

We used high-speed video tracking to quantify the axial body strain during escape twitches (STAR Methods). The strains were 5 dpf, 10.2%, and 7 dpf, 7.8% (2 dpf not quantified due to different imaging parameters; STAR Methods). Motion at 5 dpf

always exceeded a strain of 6.5% and was generally accompanied by Ca^{2+} transients (Figure 1G). We did not observe a significant correlation between strain and GCaMP fluorescence at 5 dpf, likely due to the limited range of strains observed (Spearman r = -0.21, p = 0.43). At 7 dpf, the body strain had a wider range (Figure S1), and we observed a correlation between strain and GCaMP fluorescence response (r = 0.64, p = 1.8e-3).

A previous report described elevation in basal Ca²⁺ levels in embryonic zebrafish ECs, induced by hemodynamic deflection of primary cilia. That effect did not include Ca²⁺ dynamics on the timescale of seconds, and the effect disappeared by 48 h post fertilization (hpf) due to disassembly of cilia. P,22 The bodymotion-induced Ca²⁺ transients described here appear to be a distinct phenomenon.



Skeletal muscle contraction directly triggers EC Ca²⁺ transients

We next sought to identify the biophysical and molecular pathways that led to these motion-associated EC Ca²⁺ transients. We first examined the necessity and sufficiency of different physiological dynamics involved in zebrafish swimming motion: (1) motor circuit neural activity, (2) cardiac function, and (3) skeletal muscle contraction.

We simultaneously imaged Ca^{2+} activity in ECs and in glutamatergic excitatory interneurons of the spinal cord during violet light visual stimulus using Tg(kdrl:Gal4;vglut2a:Gal4;UAS:G-CaMP6s) fish.²³ Spinal glutamatergic interneurons synapse onto cholinergic motor neurons and are a common proxy for neural motor activation in larval zebrafish.^{24,25} Violet light (405 nm) illumination of the eyes in 5 dpf larvae for 10 s elicited Ca^{2+} elevation in spinal glutamatergic neurons (98% of trials), twitch responses (98% of trials), and EC Ca^{2+} events (89% of trials; n=9 fish, 54 total trials; Figures 2B–2D; Video S1).

To assess whether neural activity alone could evoke EC Ca^{2+} events, we applied tubocurarine (TC, 2.2 mM), which blocks nicotinic acetylcholine receptors (nAchRs) and thus disrupts signal transmission across neuromuscular junctions. In the presence of TC, we still observed neural Ca^{2+} responses to 100% of stimuli (n=4 fish, 24 total trials), but we detected neither physical twitch responses nor intersegmental EC Ca^{2+} responses (Figures 2B–2D; Video S1). Larvae treated with TC showed small EC Ca^{2+} fluctuations, localized to the junction between intersegmental arteries and the DA (Video S1), which were also present in control larvae. These fluctuations were smaller in magnitude and distinct in timing and location compared with the motion-induced EC Ca^{2+} transients and appeared uncorrelated with visual stimulus (Figure S2). Due to their clear differences from the motion-evoked events, we did not analyze them further.

In TC-treated fish, the amplitude of the neural Ca²⁺ response was smaller, on average, than that in drug-free controls, perhaps because of the absence of somatosensory feedback (Figure S2). Nonetheless, comparing events of matched spinal Ca²⁺ amplitude, the EC Ca²⁺ response remained significantly smaller in the TC-treated fish than in the drug-free controls (p = 1.3e-4, mixed-effects general linear model; Figure S2). Together, these observations show that spinal motor circuit activity alone was insufficient to evoke EC Ca²⁺ transients.

A further possibility is that electrical excitation of skeletal muscles somehow activated EC Ca²⁺ transients, even in the absence of motion. To test this possibility, we applied para-amino blebbistatin (pAB, 50 μM), a photostable myosin II inhibitor that blocks muscle contraction²⁶ without impairing muscle electrical excitation. This drug partially suppressed spinal Ca²⁺ responses (responses observed in 27/46 trials, n = 8 fish) and was only partially effective at blocking twitches (twitches observed in 19/46 trials, all accompanied by spinal Ca²⁺ responses; Figures 2B-2D; Video S1). This partial efficacy allowed the observation of distinct combinations of spinal activity and twitching. EC Ca2+ responses occurred in 11/19 of the trials that evoked twitches, and not in any of the 8 trials that evoked spinal Ca2+ activity but no twitches, nor in any of the 19 trials that evoked no spinal Ca2+ activity (and no twitches). These results confirm the necessity of twitches for EC Ca2+ responses (Figures 2E and S2). The lower probability of twitch-evoked EC Ca²⁺ in the presence vs. absence of pAB is likely because pAB led to weaker and smaller twitches.

Mechanical deformation of blood vessels directly induces EC Ca²⁺ transients

The myosin inhibitor pAB also severely disrupted the heartbeat, largely eliminating resting blood flow (Video S2). Persistence of the EC Ca²⁺ events in the absence of cardiac-driven circulation implies that neither circulating endocrine factors nor changes in vessel mechanical forces driven by cardiac output were required for motion-induced EC Ca2+ events. Nonetheless, muscle motion induced some blood flow, even in the absence of cardiac output, so we asked to what extent EC Ca2+ events were evoked by motion-induced blood flow vs. by direct action of the muscles on the vasculature. We measured blood flow via high-speed video tracking of individual blood cells (Figures 3A and 3B; Video S2). In unperturbed fish at rest, the basal cardiac-driven flow in the DA was 2800 µm/s (median; 1,890-2,860 μ m/s IQR; n = 9 fish). After we eliminated cardiac output by applying 30 μM pAB (Video S2), the basal flow ceased (Video S2), but during twitches, the transient flow relative to the body rose to 2,270 (1,422–2,896) μ m/s (n = 9 fish), not significantly different (p = 0.659) from the basal flow in the unperturbed fish at rest (Figure 3C). EC Ca²⁺ transients arose during twitches in pAB-treated fish and were rare at rest in both control and pABtreated fish (Figures 1, 2, and S2). As the blood flow rates were similar in these two conditions, we infer that absolute blood flow rates contributed little to the EC Ca2+ transients. However, it remains possible that changes in flow rate or disturbed flow contributed to the EC Ca2+ response.

We then tested whether direct application of mechanical forces could induce EC Ca²⁺ transients. We treated 5 dpf fish with the voltage-gated sodium channel blocker tricaine (120 mg/L), to eliminate neural activity, and then embedded the fish in agarose. We placed a 10 g weight on top (Video S3) and quantified the Ca²⁺ response 15 s after application of the weight (to allow sufficient time for motion artifacts to subside, Figure 3D). Application of the weight-evoked Ca²⁺ increases in ECs but not in glutamatergic neurons in *Tg*(*vg*]*ut*2*a*:*Ga*1*4*;*VAS*:*Ga*1*4*;*VAS*:*GCaMP6s*) fish (Figure 3E). Control experiments in fish with a Ca²⁺-insensitive EC tag Tg(*kdrl*:*GFP*) confirmed that the weight-induced fluorescence response was not due to motion artifacts (Figure S3). Thus, force application can directly evoke EC Ca²⁺ elevation in the absence of neural activity.

We then added 2-aminoethoxydiphenyl borate (2-APB, 20 μ M) to suppress Ca²+ release from the endoplasmic reticulum and store-operated Ca²+ entry. This treatment reduced the weight-evoked Δ F/F (Figures 3E–3G; Video S3) from 0.34 (0.06–0.81) to 0.08 (–0.05 to 0.29) (p = 0.062; n = 11 fish control, n = 13 fish 2-APB), suggesting that the weight-evoked transients engage Ca²+ release from intracellular stores (e.g., via inositol-triphosphate receptors²7 and/or ORAl1²8).

Piezo1 is required for mechano-activated EC Ca²⁺

We next sought to identify the molecular mechanosensor that initiates the EC Ca²⁺ responses. ECs express several plasma membrane mechanosensitive Ca²⁺ ion channels. We selected three mechanosensitive ion channels as candidates, based on



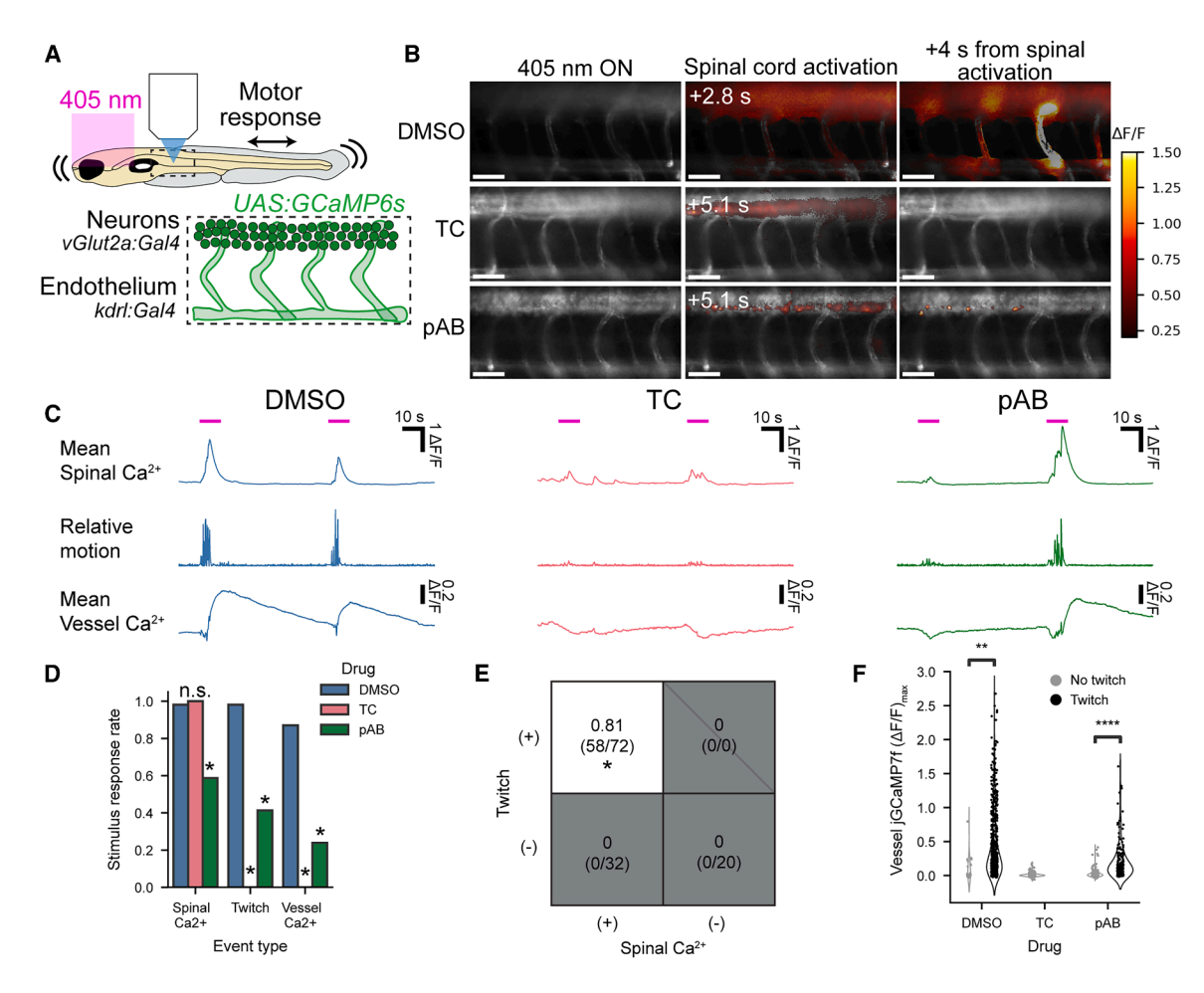


Figure 2. Calcium events in ECs require muscle contraction

- (A) Experimental setup. Violet light on the eyes evoked escape attempts; Ca²⁺ responses were monitored in the spinal cord and in vascular ECs.
- (B) Representative twitch-evoked Ca²⁺ response maps upon treatment with vehicle control (0.3% DMSO), 2.2 mM tubocurarine (TC), or 50 μM para-amino blebbistatin (pAB). Scale bars, 50 μm.
- (C) Typical visual-stimulus-evoked response waveforms. The negative-going transients in the vessel Ca²⁺ signals are motion artifacts.
- (D) Probability that a visual-stimulus-evoked different measures of response (spinal Ca²⁺, twitch, or vessel Ca²⁺).
- (E) Probability of EC Ca²⁺ transients conditional on twitch and spinal Ca²⁺ responses, aggregated across all pharmacological treatments. Events with spinal Ca²⁺ but no twitch did not evoke EC Ca²⁺ transients, while events with twitch-evoked EC Ca²⁺ transients with 81% probability.
- (F) Maximum vessel Δ F/F triggered on motion. Each point is one vessel during one visual stimulus (DMSO, 680 vessel events; TC, 320 vessel events; pAB, 448 vessel events).
- (D-F) n = 9 fish DMSO, 4 fish TC, and 8 fish pAB.

Statistical tests: (D) mixed-effects linear model considering individual fish and treatment. Spinal Ca^{2+} : TC, p=0.91, z=0.11; pAB, p=4.3e-3, z=-2.9. Motion: TC, p=8.7e-12, z=-6.8; pAB, p=2.4e-6, z=-4.7. Vessel Ca^{2+} : TC, p=8.5e-12, z=-6.8; pAB, p=1.6e-9, z=-6.0. (E) Mixed-effects linear model considering the separate effects of spinal Ca^{2+} and motion as well as individual fish on each vessel. Spinal Ca^{2+} , p=0.29; motion, p=8.7e-17. (F) Mixed-effect linear model considering effects of drug and individual fish on each vessel. DMSO, z=3.0, p=3.2e-3; pAB, z=9.6, p=8.1e-22. Additional supporting data in Figure S2.

Ca²⁺ permeability, sub-second response kinetics,^{29–31} and previously documented expression in ECs^{20,30,32}: Piezo1, PKD2, and TRPV4. We performed CRISPR-Cas9-mediated knockout (KO) of these channels at the single-cell stage. We validated cutting of genomic DNA in each experiment by gel electrophoresis and sequencing (Figure S4). We measured EC Ca²⁺ events in each KO during electric-field stimulus-evoked body motions in live fish.

Single-guide RNAs (sgRNAs) targeting *piezo1* diminished protein expression, as quantified by western blot (Figure 4A). In *Tg(kdrl:Gal4; UAS:GCaMP5G)* fish with *piezo1* KO, we observed

significantly diminished motion-triggered EC Ca²⁺ events (Figure 4B). In contrast, uninjected fish showed normal motion-triggered EC Ca²⁺ events (Figures 4B–4D). *pkd2* and *trpv4* KO fish had no detectable difference in motion-triggered EC Ca²⁺ events compared with uninjected controls (Figures 4B–4D).

In mice, endothelium-specific Piezo1 deficiency has been reported to cause defects in vascular development and embryonic lethality: Piezo1^{-/-} mice embryos die mid-gestation at embryonic day (E)9.5.^{10,17} To control for possible developmental defects resulting from chronic Piezo1 deficiency in the CRISPR-Cas9 KOs, we treated non-KO fish with pharmacological



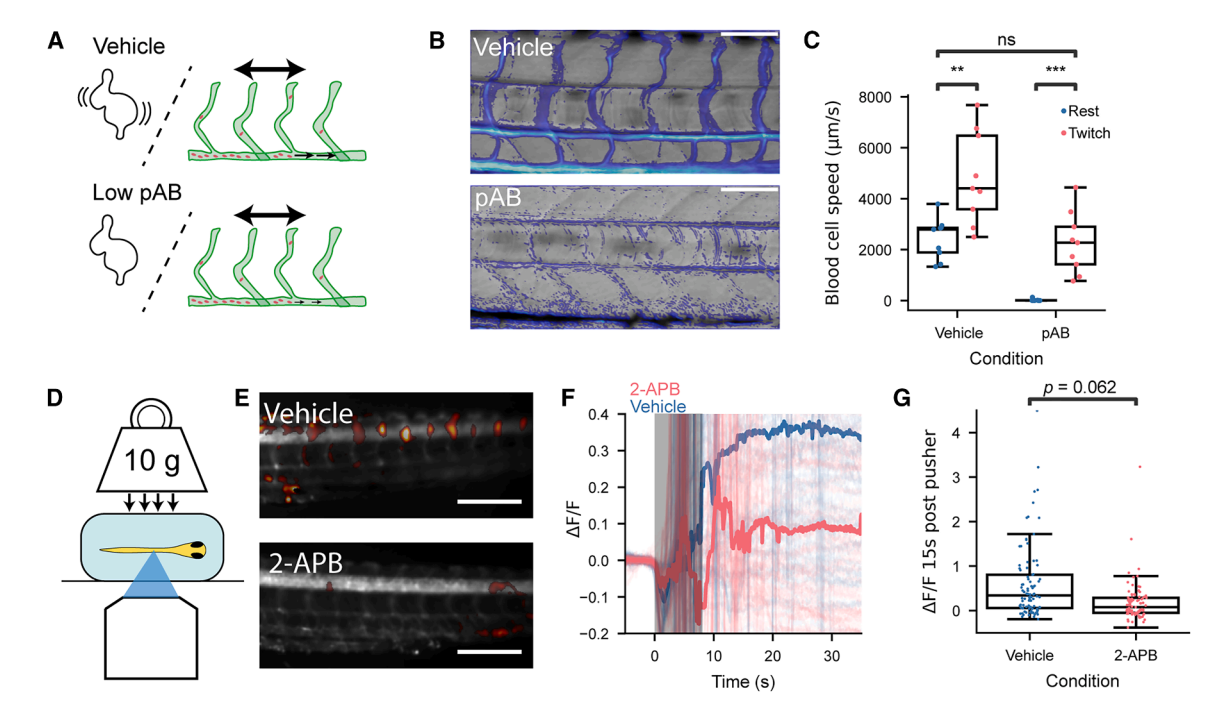


Figure 3. Blood vessel deformation directly induces Ca²⁺ events in ECs

(A) Schematic showing effect of 30 μM para-amino blebbistatin (pAB) on cardiac contractility, blood flow, and body motion.

(B) Bright-field-transmitted light movies were used to quantify blood flow. Composite image showing average image (gray) and speckle amplitude (color), caused by flowing blood cells. Treatment with pAB stopped the heartbeat (Video S2) and largely suppressed cardiac-driven blood flow.

(C) DA blood cell velocity in vehicle (0.3% DMSO) and pAB treatment.

(A–C) n = 9 fish vehicle, n = 9 fish pAB.

(D) Schematic of weight press experiment.

(E) Example ΔF/F at 15 s after press for Tg(kdrl:Gal4;vglut2a:Gal4;UAS:GCaMP6s) fish treated with vehicle (0.3% DMSO) or 20 μM 2-aminoethoxydiphenyl borate (2-APB).

(F) Fluorescence response vs. time relative to weight push. Solid lines are median over individual vessels. Initial response is dominated by motion associated with application of the weight (shaded region).

(G) Fluorescence response 15 s after weight application.

(F and G) 92 vessels from n=11 fish vehicle, 93 vessels from n=13 fish 2-APB.

Statistical tests: (A–C) Mann-Whitney-Wilcoxon two-sided test. Twitch vs. rest (vehicle), p = 6.2e - 3, U = 9.0; twitch vs. rest (pAB), p = 4.1e - 4, U = 0; rest (vehicle) vs. twitch (pAB), p = 0.66, U = 46.0. (F and G) Mixed-effect linear model considering the effects of 2-APB and individual fish, p = 0.062, z = -1.9. Additional supporting data in Figure S3.

See also Video S3.

blockers of Piezo1: ruthenium red, Gd³⁺, streptomycin, or GsMTx-4^{21,33} (STAR Methods). However, these drugs all induced lethality before inhibiting visual stimulus- or weight-evoked EC Ca²⁺ transients. We speculate that residual channel activity under partial pharmacological block may have been sufficient to initiate calcium-induced calcium release from intracellular stores (Figure S3).

As an alternative approach, we selectively knocked down piezo1 in zebrafish at 3 dpf using a photo-cleavable, translation-blocking morpholino (photo-MO; Figure 4E). Embryos were injected with the photo-MO at the single-cell stage and exposed to 355 nm laser at 3 dpf (Figure 4F). Western blot analysis confirmed Piezo1 knockdown (KD) in treated fish (Figure 4G). All piezo1 morphants showed normal vascular morphology with no noticeable developmental defects. By 5 dpf, we found that piezo1 morphants showed reduced EC Ca^{2+} events following body twitching (Figure 4H). We found a positive correlation between EC Ca^{2+} transient amplitudes and Piezo1 protein levels measured in the same fish ($R^2 = 0.49$,

Figure 4I). These data are consistent with the interpretation that Piezo1 mediates rapid mechanically induced Ca²⁺ events in ECs of zebrafish *in vivo*, although it is also possible that loss of Piezo1 from 3 to 5 dpf led to suppression of EC Ca²⁺ events through an indirect mechanism.

DISCUSSION

We demonstrated a direct mechanical coupling between physical tissue motion and EC Ca²⁺ signaling *in vivo*, mediated by the Piezo1 mechanosensitive ion channel. Basal blood flow alone was not sufficient to trigger these Ca²⁺ events, while swimming-induced motions or externally applied compression induced these events even in the absence of heartbeat-driven circulation.

Mechanotransduction in vasculature has been implicated in regulating vascular tone, primarily through sensing changes in blood flow directly or consequent changes in oxygenation. ^{34,35} Changes in vascular tone have been observed as rapidly as a



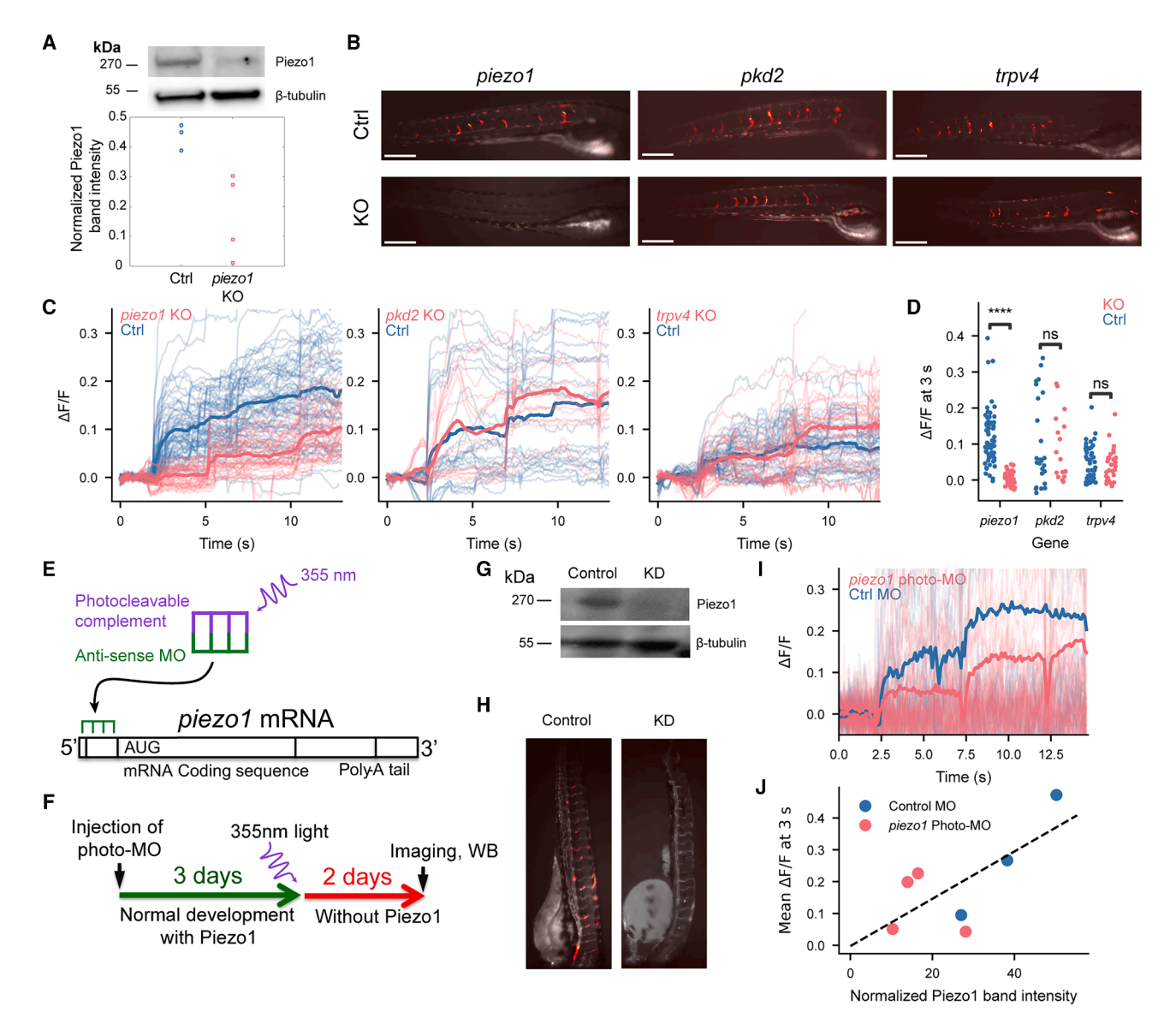


Figure 4. Piezo1 channels are required for motion-evoked EC Ca²⁺ events

- (A) Western blot quantification of Piezo1 expression in whole-animal lysates from control and Piezo1 gRNA-injected fish (5 dpf), normalized to β-tubulin band intensity.
- (B) Relative GCaMP5G fluorescence 3 s after electrical field stimulus in KO (piezo1, pkd2, or trpv4) versus control Tg(kdrl:Gal4;UAS:GCaMP5G) fish. Scale bars, 500 μm.
- (C) Δ F/F traces for individual blood vessel segments. Electric-field stimuli at 2, 6, and 11 s. Bold lines indicate mean over all measured vessels in each group of fish.
- (D) $\Delta F/F$ 3 s after the first electrical field stimulus.
- (C and D) n = 6 controls, n = 3 KO piezo1; n = 3 controls, n = 3 KO pkd2; n = 4 controls, n = 3 KO trpv4.
- (E) Photo-morpholino (MO) mechanism of action.
- (F) Experimental design for temporally restricted photo-MO KD of Piezo1.
- (G) Western blot measuring Piezo1 KD by photo-MO.
- (H) Relative GCaMP5G fluorescence 3 s after electrical field stimulus in scrambled and piezo1 photo-MO-treated fish.
- (I) Δ F/F traces for individual blood vessel segments. Bold line represents the mean over all measured vessels.
- (J) Mean GCaMP5G Δ F/F over ISVs 3 s after electrical field stimulus compared with post hoc western blot Piezo1 band intensity normalized to β -tubulin band intensity (Pearson $R^2 = 0.49$).
- (I and J) Control MO: 34 vessels over n=3 fish, piezo1 photo-MO 68 vessels over n=4 fish.
- Statistical tests: (D) mixed-effects linear model considering individual fish and CRISPR-Cas9 treatment of each vessel. piezo1, z = -4.8, p = 1.4e-6; pkd2, z = 0.48, p = 0.63; trpv4, z = 0.002, p = 0.998. Additional supporting data in Figure S4.



single muscular contraction (\sim 1 s or less), $^{36-41}$ and in response to externally applied forces, leading some to propose that local mechanical compression of vessels may also play a role. 41,42 Here, we show that EC compression by muscle action or external force is directly sensed by Piezo1, providing a molecular mechanism of triggering rapid cellular responses to local mechanical forces.

The overall function of Piezo1 in vascular physiology remains uncertain, and it may serve multiple roles. Ca²⁺ entry in ECs induces vasodilatory responses by activating synthesis of nitric oxide⁴³ and through hyperpolarization via calcium-activated potassium channels.^{44,45} On the other hand, Piezo1 activation directly provides a depolarizing cation current, which may counteract endothelial hyperpolarization-induced vascular smooth muscle cell (VSMC) relaxation.^{45–47}

In mice, Piezo1 contributes to higher systemic blood pressure during exercise and to vasoconstriction in mesenteric resistance arteries (when NO synthesis is blocked).46 Similarly, Piezo1mediated depolarization serves as a brake on neuronal-activity-induced hyperemia in the brain vasculature. 47 In contrast, arteriolar dilation upon hamster cremaster muscle contraction requires EC Ca²⁺ elevation.⁴⁸ We used a spinning disk confocal microscope to track EC Ca2+ and vessel diameter during visualstimulus-evoked twitches in 7 dpf fish. We observed no significant changes in ISV diameter (data available upon request). We observed motion-related dilation in the DA, but these changes did not correlate with local calcium increases. It is possible that the changes in EC Ca2+ could act through a nonlocal mechanism, such as conducted vasodilation, 49 but that idea remains speculative. It is also possible that the coupling of EC Ca²⁺ to vasodilation is not fully active at 7 dpf⁵⁰ or that vasodilation is triggered independent of EC Ca2+. Indeed, compression-induced vasodilation has been reported in ECdenuded vessels.41

In embryonic development, forces related to blood flow are important for angiogenesis, 9,10,17 cardiac valve and endocardium development, 51 VSMC differentiation and arterial vasculature stabilization, ^{52,53} and hematopoietic stem cell induction and expansion. ^{54,55} Piezo1 is implicated in the transduction of these forces. 10,17,53,55 Our findings suggest that Piezo1 could integrate information on body motion that emerges during development. We pharmacologically arrested body motion from 2 to 5 dpf but did not observe effects on vascular diameter, architecture, or coverage of vascular mural cells at 5 dpf (data available upon request). The downstream biological functions of the observed Ca²⁺ transients remain to be discovered. For instance, body motion may play a role in other processes we did not examine or may have effects later in life. At a longer timescale, endothelial Piezo1 might also sense local forces exerted by neighboring tissues during morphogenesis.⁵⁶ Our work highlights the importance of mapping molecular mechanisms of mechanosensation in the context of physiological body forces.

RESOURCE AVAILABILITY

Lead contact

Requests for resources, reagents, or data should be directed to the lead contact, Adam Cohen (cohen@chemistry.harvard.edu).

Materials availability

All requests for transgenic zebrafish lines will be fulfilled by the lead contact, Adam Cohen (cohen@chemistry.harvard.edu).

Data and code availability

- All analysis code (described in STAR Methods) is on Zenodo: 10.5281/ zenodo.17330879.
- All raw imaging data are available from the lead contact upon request.
- Any additional information required to reanalyze the data reported in this
 paper is available from the lead contact upon request.

ACKNOWLEDGMENTS

This work was supported by funds from Harvard University and the Howard Hughes Medical Institute (HHMI). We thank Calum A. MacRae for the gift of the *Tg(kdrl:Gal4)* line. We thank Luis Hernandez-Nunez for the gift of the *Tg(kdrl:eGFP)* line. We thank Jennifer Hou, Christopher A. Werley, Peng Zou, James Lee, Erin Yue Song, Eva Fast, Joel M. Kralj, and Adam Douglass for helpful discussions and training. We gratefully acknowledge help from members of the labs of A.E.C., F.E., Alex Schier, and Leonard Zon. F.E. received funding from the National Institutes of Health (U19NS104653 and 1R01NS124017-01), DoD (W911NF2420112), and Simons Foundation (SCGB 542973 and NC-GB-CULM-00003241-02). This work was supported by funding from the National Heart, Lung, and Blood Institute (1P01HL131477) and the National Institute of Diabetes and Digestive and Kidney Diseases (R01 DK140372) to L.I.Z.

AUTHOR CONTRIBUTIONS

A.E.C. and X.T. conceptualized the work. X.T. performed initial characterization of the EC Ca²⁺ mechano-response and designed, executed, and analyzed the experiment for Figure 4, with assistance from M.P.R. B.Z.J. designed, executed, and analyzed experiments for all other figures. L.I.Z. and F.E. provided zebrafish lines and guidance on experimental design. B.Z.J., X.T., and A.E.C. wrote the manuscript, with input from all authors.

DECLARATION OF INTERESTS

The authors declare no competing interests.

STAR*METHODS

Detailed methods are provided in the online version of this paper and include the following:

- KEY RESOURCES TABLE
- EXPERIMENTAL MODEL AND STUDY PARTICIPANT DETAILS
 - Zebrafish
 ∴
 ✓
 ✓
 ✓
 ✓
 ✓
 ✓
 ✓
 ✓
 ✓
 ✓
 ✓
 ✓
 ✓
 ✓
 ✓
 ✓
 ✓
 ✓
 ✓
 ✓
 ✓
 ✓
- METHOD DETAILS
 - o Microscopy and imaging
 - Visual stimulation to evoke twitch responses
 - o Mechanical compression of larvae
 - Electrical stimulation of fish motion
 - Pharmacological treatments
 - o CRISPR/Cas9 knockouts
 - o Morpholino/Photo-morpholino knockdown
 - Western blot analysis
 - o Fluorescence in situ hybridization (HCR-FISH)
- QUANTIFICATION AND STATISTICAL ANALYSIS

SUPPLEMENTAL INFORMATION

Supplemental information can be found online at https://doi.org/10.1016/j.cub.2025.10.053.

Received: February 6, 2025 Revised: August 26, 2025 Accepted: October 16, 2025



REFERENCES

- Davis, M.J., Earley, S., Li, Y.-S., and Chien, S. (2023). Vascular mechanotransduction. Physiol. Rev. 103, 1247–1421. https://doi.org/10.1152/physrev.00053.2021.
- Hahn, C., and Schwartz, M.A. (2009). Mechanotransduction in vascular physiology and atherogenesis. Nat. Rev. Mol. Cell Biol. 10, 53–62. https://doi.org/10.1038/nrm2596.
- Pober, J.S., and Sessa, W.C. (2007). Evolving functions of endothelial cells in inflammation. Nat. Rev. Immunol. 7, 803–815. https://doi.org/10.1038/ pri/2171
- Lopez-Crisosto, C., Pennanen, C., Vasquez-Trincado, C., Morales, P.E., Bravo-Sagua, R., Quest, A.F.G., Chiong, M., and Lavandero, S. (2017). Sarcoplasmic reticulum-mitochondria communication in cardiovascular pathophysiology. Nat. Rev. Cardiol. 14, 342–360. https://doi.org/10. 1038/nrcardio.2017.23.
- Olesen, S.P., Clapham, D.E., and Davies, P.F. (1988). Haemodynamic shear stress activates a K+ current in vascular endothelial cells. Nature 331, 168–170. https://doi.org/10.1038/331168a0.
- Tzima, E., del Pozo, M.A., Shattil, S.J., Chien, S., and Schwartz, M.A. (2001). Activation of integrins in endothelial cells by fluid shear stress mediates Rho-dependent cytoskeletal alignment. EMBO J. 20, 4639–4647. https://doi.org/10.1093/emboj/20.17.4639.
- Lu, D., and Kassab, G.S. (2011). Role of shear stress and stretch in vascular mechanobiology. J. R. Soc. Interface 8, 1379–1385. https://doi. org/10.1098/rsif.2011.0177.
- Yamashiro, Y., and Yanagisawa, H. (2020). The molecular mechanism of mechanotransduction in vascular homeostasis and disease. Clin. Sci. (Lond) 134, 2399–2418. https://doi.org/10.1042/CS20190488.
- Goetz, J.G., Steed, E., Ferreira, R.R., Roth, S., Ramspacher, C., Boselli, F., Charvin, G., Liebling, M., Wyart, C., Schwab, Y., et al. (2014). Endothelial cilia mediate low flow sensing during zebrafish vascular development. Cell Rep. 6, 799–808. https://doi.org/10.1016/j.celrep.2014.01.032.
- Li, J., Hou, B., Tumova, S., Muraki, K., Bruns, A., Ludlow, M.J., Sedo, A., Hyman, A.J., McKeown, L., Young, R.S., et al. (2014). Piezo1 integration of vascular architecture with physiological force. Nature 515, 279–282. https://doi.org/10.1038/nature13701.
- Dai, G., Kaazempur-Mofrad, M.R., Natarajan, S., Zhang, Y., Vaughn, S., Blackman, B.R., Kamm, R.D., García-Cardeña, G., and Gimbrone, M.A. (2004). Distinct endothelial phenotypes evoked by arterial waveforms derived from atherosclerosis-susceptible and -resistant regions of human vasculature. Proc. Natl. Acad. Sci. USA 101, 14871–14876. https://doi. org/10.1073/pnas.0406073101.
- Wang, S., Iring, A., Strilic, B., Albarrán Juárez, J.A., Kaur, H., Troidl, K., Tonack, S., Burbiel, J.C., Müller, C.E., Fleming, I., et al. (2015). P2Y2 and Gq/G11 control blood pressure by mediating endothelial mechanotransduction. J. Clin. Invest. 125, 3077–3086. https://doi.org/10.1172/ JCI81067
- Barakat, A.I., Leaver, E.V., Pappone, P.A., and Davies, P.F. (1999). A flow-activated chloride-selective membrane current in vascular endothelial cells. Circ. Res. 85, 820–828. https://doi.org/10.1161/01.RES.85.9.820.
- Oteiza, P., Odstrcil, I., Lauder, G., Portugues, R., and Engert, F. (2017). A novel mechanism for mechanosensory-based rheotaxis in larval zebrafish. Nature 547, 445–448. https://doi.org/10.1038/nature23014.
- Chien, S. (2007). Mechanotransduction and endothelial cell homeostasis: the wisdom of the cell. Am. J. Physiol. Heart Circ. Physiol. 292, H1209– H1224. https://doi.org/10.1152/ajpheart.01047.2006.
- Feaver, R.E., Gelfand, B.D., and Blackman, B.R. (2013). Human haemodynamic frequency harmonics regulate the inflammatory phenotype of vascular endothelial cells. Nat. Commun. 4, 1525. https://doi.org/10. 1038/ncomms2530.
- Ranade, S.S., Qiu, Z., Woo, S.-H., Hur, S.S., Murthy, S.E., Cahalan, S.M., Xu, J., Mathur, J., Bandell, M., Coste, B., et al. (2014). Piezo1, a mechanically activated ion channel, is required for vascular development in mice.

- Proc. Natl. Acad. Sci. USA 111, 10347–10352. https://doi.org/10.1073/pnas.1409233111.
- Chen, T.-W., Wardill, T.J., Sun, Y., Pulver, S.R., Renninger, S.L., Baohan, A., Schreiter, E.R., Kerr, R.A., Orger, M.B., Jayaraman, V., et al. (2013). Ultrasensitive fluorescent proteins for imaging neuronal activity. Nature 499, 295–300. https://doi.org/10.1038/nature12354.
- Guggiana-Nilo, D.A., and Engert, F. (2016). Properties of the visible light phototaxis and UV avoidance behaviors in the larval zebrafish. Front. Behav. Neurosci. 10, 160. https://doi.org/10.3389/fnbeh.2016.00160.
- Hartmannsgruber, V., Heyken, W.-T., Kacik, M., Kaistha, A., Grgic, I., Harteneck, C., Liedtke, W., Hoyer, J., and Köhler, R. (2007). Arterial response to shear stress critically depends on endothelial TRPV4 expression. PloS One 2, e827. https://doi.org/10.1371/journal.pone.0000827.
- Bae, C., Sachs, F., and Gottlieb, P.A. (2011). The mechanosensitive ion channel Piezo1 is inhibited by the peptide GsMTx4. Biochemistry 50, 6295–6300. https://doi.org/10.1021/bi200770q.
- Iomini, C., Tejada, K., Mo, W., Vaananen, H., and Piperno, G. (2004).
 Primary cilia of human endothelial cells disassemble under laminar shear stress. J. Cell Biol. 164, 811–817. https://doi.org/10.1083/jcb.200312133.
- Satou, C., Kimura, Y., Hirata, H., Suster, M.L., Kawakami, K., and Higashijima, S. (2013). Transgenic tools to characterize neuronal properties of discrete populations of zebrafish neurons. Development *140*, 3927–3931. https://doi.org/10.1242/dev.099531.
- Wahlstrom-Helgren, S., Montgomery, J.E., Vanpelt, K.T., Biltz, S.L., Peck, J.H., and Masino, M.A. (2019). Glutamate receptor subtypes differentially contribute to optogenetically activated swimming in spinally transected zebrafish larvae. J. Neurophysiol. 122, 2414–2426. https://doi.org/10. 1152/jn.00337.2019.
- Böhm, U.L., Kimura, Y., Kawashima, T., Ahrens, M.B., Higashijima, S.I., Engert, F., and Cohen, A.E. (2022). Voltage imaging identifies spinal circuits that modulate locomotor adaptation in zebrafish. Neuron 110, 1211–1222.e4. https://doi.org/10.1016/j.neuron.2022.01.001.
- Várkuti, B.H., Képiró, M., Horváth, I.Á., Végner, L., Ráti, S., Zsigmond, Á., Hegyi, G., Lenkei, Z., Varga, M., and Málnási-Csizmadia, A. (2016). A highly soluble, non-phototoxic, non-fluorescent blebbistatin derivative. Sci. Rep. 6, 26141. https://doi.org/10.1038/srep26141.
- Maruyama, T., Kanaji, T., Nakade, S., Kanno, T., and Mikoshiba, K. (1997).
 2APB, 2-aminoethoxydiphenyl borate, a membrane-penetrable modulator of Ins(1,4,5)P3-induced Ca2+ release. J. Biochem. 122, 498–505. https://doi.org/10.1093/oxfordjournals.jbchem.a021780.
- Wei, M., Zhou, Y., Sun, A., Ma, G., He, L., Zhou, L., Zhang, S., Liu, J., Zhang, S.L., Gill, D.L., et al. (2016). Molecular mechanisms of inhibition on STIM1-Orai1 mediated Ca²⁺ entry induced by 2-aminoethoxydiphenyl borate. Pflugers Arch. 468, 2061–2074. https://doi.org/10.1007/s00424-016-1880-z.
- Gnanasambandam, R., Gottlieb, P.A., and Sachs, F. (2017). The kinetics and the permeation properties of Piezo channels. Curr. Top. Membr. 79, 275–307. https://doi.org/10.1016/bs.ctm.2016.11.004.
- AbouAlaiwi, W.A., Takahashi, M., Mell, B.R., Jones, T.J., Ratnam, S., Kolb, R.J., and Nauli, S.M. (2009). Ciliary polycystin-2 is a mechanosensitive calcium channel involved in nitric oxide signaling cascades. Circ. Res. 104, 860–869. https://doi.org/10.1161/CIRCRESAHA.108.192765.
- Gao, X., Wu, L., and O'Neil, R.G. (2003). Temperature-modulated diversity
 of TRPV4 channel gating: activation by physical stresses and phorbol
 ester derivatives through protein kinase C-dependent and -independent
 pathways. J. Biol. Chem. 278, 27129–27137. https://doi.org/10.1074/
 ibc.M302517200.
- Heckel, E., Boselli, F., Roth, S., Krudewig, A., Belting, H.-G., Charvin, G., and Vermot, J. (2015). Oscillatory flow modulates mechanosensitive klf2a expression through trpv4 and trpp2 during heart valve development. Curr. Biol. 25, 1354–1361. https://doi.org/10.1016/j.cub.2015.03.038.
- 33. Coste, B., Mathur, J., Schmidt, M., Earley, T.J., Ranade, S., Petrus, M.J., Dubin, A.E., and Patapoutian, A. (2010). Piezo1 and Piezo2 are essential



- components of distinct mechanically activated cation channels. Science 330, 55–60. https://doi.org/10.1126/science.1193270.
- Mohrman, D.E., and Sparks, H.V. (1974). Myogenic hyperemia following brief tetanus of canine skeletal muscle. Am. J. Physiol. 227, 531–535. https://doi.org/10.1152/ajplegacy.1974.227.3.531.
- Messere, A., Ceravolo, G., Franco, W., Maffiodo, D., Ferraresi, C., and Roatta, S. (2017). Increased tissue oxygenation explains the attenuation of hyperemia upon repetitive pneumatic compression of the lower leg. J. Appl. Physiol. (1985) 123, 1451–1460. https://doi.org/10.1152/japplphysiol.00511.2017.
- Anrep, G., Blalock, A., and Samaan, A. (1934). The effect of muscular contraction upon the blood flow in the skeletal muscle. Proc. R. Soc. Lond. B. 114, 223–245. https://doi.org/10.1098/rspb.1934.0003.
- Buckwalter, J.B., Ruble, S.B., Mueller, P.J., and Clifford, P.S. (1998).
 Skeletal muscle vasodilation at the onset of exercise. J. Appl. Physiol. (1985) 85, 1649–1654. https://doi.org/10.1152/jappl.1998.85.5.1649.
- Naik, J.S., Valic, Z., Buckwalter, J.B., and Clifford, P.S. (1999). Rapid vasodilation in response to a brief tetanic muscle contraction. J. Appl. Physiol. (1985) 87, 1741–1746. https://doi.org/10.1152/jappl.1999.87.5.1741.
- VanTeeffelen, J.W.G.E., and Segal, S.S. (2006). Rapid dilation of arterioles with single contraction of hamster skeletal muscle. Am. J. Physiol. Heart Circ. Physiol. 290, H119-H127. https://doi.org/10.1152/ajpheart. 00197.2005.
- Crecelius, A.R., Kirby, B.S., Luckasen, G.J., Larson, D.G., and Dinenno, F.A. (2013). Mechanisms of rapid vasodilation after a brief contraction in human skeletal muscle. Am. J. Physiol. Heart Circ. Physiol. 305, H29–H40. https://doi.org/10.1152/ajpheart.00298.2013.
- Clifford, P.S., Kluess, H.A., Hamann, J.J., Buckwalter, J.B., and Jasperse, J.L. (2006). Mechanical compression elicits vasodilatation in rat skeletal muscle feed arteries. J. Physiol. 572, 561–567. https://doi.org/10.1113/ jphysiol.2005.099507.
- Lu, X., and Kassab, G.S. (2015). Integrins mediate mechanical compression-induced endothelium-dependent vasodilation through endothelial nitric oxide pathway. J. Gen. Physiol. 146, 221–232. https:// doi.org/10.1085/jgp.201411350.
- Fleming, I., and Busse, R. (2003). Molecular mechanisms involved in the regulation of the endothelial nitric oxide synthase. Am. J. Physiol. Regul. Integr. Comp. Physiol. 284, R1–R12. https://doi.org/10.1152/ajpregu. 00323.2002.
- Doughty, J.M., Plane, F., and Langton, P.D. (1999). Charybdotoxin and apamin block EDHF in rat mesenteric artery if selectively applied to the endothelium. Am. J. Physiol. 276, H1107–H1112. https://doi.org/10. 1152/ajpheart.1999.276.3.H1107.
- Garland, C.J., and Dora, K.A. (2017). EDH: endothelium-dependent hyperpolarization and microvascular signalling. Acta Physiol. (Oxf) 219, 152–161. https://doi.org/10.1111/apha.12649.
- Rode, B., Shi, J., Endesh, N., Drinkhill, M.J., Webster, P.J., Lotteau, S.J., Bailey, M.A., Yuldasheva, N.Y., Ludlow, M.J., Cubbon, R.M., et al. (2017). Piezo1 channels sense whole body physical activity to reset cardiovascular homeostasis and enhance performance. Nat. Commun. 8, 350. https://doi.org/10.1038/s41467-017-00429-3.
- Lim, X.R., Abd-Alhaseeb, M.M., Ippolito, M., Koide, M., Senatore, A.J., Plante, C., Hariharan, A., Weir, N., Longden, T.A., Laprade, K.A., et al. (2024). Endothelial Piezo1 channel mediates mechano-feedback control of brain blood flow. Nat. Commun. 15, 8686. https://doi.org/10.1038/ s41467-024-52969-0.
- Murrant, C.L., Duza, T., Kim, M.B., Cohen, K.D., and Sarelius, I.H. (2004).
 Arteriolar dilations induced by contraction of hamster cremaster muscle are dependent on changes in endothelial cell calcium. Acta Physiol. Scand. 180, 231–238. https://doi.org/10.1046/j.0001-6772.2003.01241.x.
- Bagher, P., and Segal, S.S. (2011). Regulation of blood flow in the microcirculation: role of conducted vasodilation. Acta Physiol. (Oxf) 202, 271–284. https://doi.org/10.1111/j.1748-1716.2010.02244.x.

- Bahrami, N., and Childs, S.J. (2020). Development of vascular regulation in the zebrafish embryo. Development 147, dev183061. https://doi.org/10. 1242/dev.183061.
- Fukui, H., Chow, R.W.-Y., Xie, J., Foo, Y.Y., Yap, C.H., Minc, N., Mochizuki, N., and Vermot, J. (2021). Bioelectric signaling and the control of cardiac cell identity in response to mechanical forces. Science 374, 351–354. https://doi.org/10.1126/science.abc6229.
- Sugden, W.W., Meissner, R., Aegerter-Wilmsen, T., Tsaryk, R., Leonard, E.V., Bussmann, J., Hamm, M.J., Herzog, W., Jin, Y., Jakobsson, L., et al. (2017). Endoglin controls blood vessel diameter through endothelial cell shape changes in response to haemodynamic cues. Nat. Cell Biol. 19, 653–665. https://doi.org/10.1038/ncb3528.
- Abello, J., Yin, Y., Zhao, Y., Maurer, J., Lee, J., Bodell, C., Richee, J., Clevenger, A.J., Burton, Z., Goeckel, M.E., et al. (2025). Endothelial cell Piezo1 promotes vascular smooth muscle cell differentiation on large arteries. Eur. J. Cell Biol. 104, 151473. https://doi.org/10.1016/j.ejcb.2024. 151473.
- North, T.E., Goessling, W., Peeters, M., Li, P., Ceol, C., Lord, A.M., Weber, G.J., Harris, J., Cutting, C.C., Huang, P., et al. (2009). Hematopoietic stem cell development is dependent on blood flow. Cell 137, 736–748. https:// doi.org/10.1016/j.cell.2009.04.023.
- Sugden, W.W., LeBlanc, Z., Tanaka-Yano, M., Jing, R., di Tillio, M.G., Najia, M., Tang, Y., Molnar, E., George, S., Love, B., et al. (2023). Blood flow directs Yap/Taz-mediated transcriptional regulation of self-renewal programs to control developmental HSPC expansion by mechanical stimulation of Piezo1. Blood 142, 1309. https://doi.org/10.1182/blood-2023-190416.
- Maroudas-Sacks, Y., and Keren, K. (2021). Mechanical patterning in animal morphogenesis. Annu. Rev. Cell Dev. Biol. 37, 469–493. https://doi.org/10.1146/annurev-cellbio-120319-030931.
- Kim, A.D., Melick, C.H., Clements, W.K., Stachura, D.L., Distel, M., Panáková, D., MacRae, C., Mork, L.A., Crump, J.G., and Traver, D. (2014). Discrete Notch signaling requirements in the specification of hematopoietic stem cells. EMBO J. 33, 2363–2373. https://doi.org/10. 15252/embj.201488784.
- Fidelin, K., Djenoune, L., Stokes, C., Prendergast, A., Gomez, J., Baradel, A., Del Bene, F., and Wyart, C. (2015). State-dependent modulation of locomotion by GABAergic spinal sensory neurons. Curr. Biol. 25, 3035– 3047. https://doi.org/10.1016/j.cub.2015.09.070.
- Muto, A., Lal, P., Ailani, D., Abe, G., Itoh, M., and Kawakami, K. (2017).
 Activation of the hypothalamic feeding centre upon visual prey detection.
 Nat. Commun. 8, 15029. https://doi.org/10.1038/ncomms15029.
- Beis, D., Bartman, T., Jin, S.-W., Scott, I.C., D'Amico, L.A., Ober, E.A., Verkade, H., Frantsve, J., Field, H.A., Wehman, A., et al. (2005). Genetic and cellular analyses of zebrafish atrioventricular cushion and valve development. Development 132, 4193–4204. https://doi.org/10.1242/dev. 01970.
- O'Brown, N.M., Patel, N.B., Hartmann, U., Klein, A.M., Gu, C., and Megason, S.G. (2023). The secreted neuronal signal Spock1 promotes blood-brain barrier development. Dev. Cell 58, 1534–1547.e6. https:// doi.org/10.1016/j.devcel.2023.06.005.
- Ferrante, M.I., Kiff, R.M., Goulding, D.A., and Stemple, D.L. (2011).
 Troponin T is essential for sarcomere assembly in zebrafish skeletal muscle. J. Cell Sci. 124, 565–577. https://doi.org/10.1242/jcs.071274.
- Itkis, D.G., Brooks, F.P., Davis, H.C., Hotter, R., Wong-Campos, J.D., Qi, Y., Jia, B.Z., Howell, M., Xiong, M., Hayward, R.F., et al. (2025). Luminos: open-source software for bidirectional microscopy. Preprint at bioRxiv. https://doi.org/10.1101/2025.02.22.639658.
- Tian, H., Davis, H.C., Wong-Campos, J.D., Park, P., Fan, L.Z., Gmeiner, B., Begum, S., Werley, C.A., Borja, G.B., Upadhyay, H., et al. (2023). Video-based pooled screening yields improved far-red genetically encoded voltage indicators. Nat. Methods 20, 1082–1094. https://doi.org/ 10.1038/s41592-022-01743-5.
- Werley, C.A., Chien, M.-P., and Cohen, A.E. (2017). Ultrawidefield microscope for high-speed fluorescence imaging and targeted optogenetic



Current Biology Report

- stimulation. Biomed. Opt. Express 8, 5794–5813. https://doi.org/10.1364/BOE.8.005794.
- Heylen, L., Pham, D.-H., De Meulemeester, A.-S., Samarut, É., Skiba, A., Copmans, D., Kazwiny, Y., Vanden Berghe, P., de Witte, P.A.M., and Siekierska, A. (2021). Pericardial injection of kainic acid induces a chronic epileptic state in larval zebrafish. Front. Mol. Neurosci. 14, 753936. https:// doi.org/10.3389/fnmol.2021.753936.
- Labun, K., Montague, T.G., Gagnon, J.A., Thyme, S.B., and Valen, E. (2016). CHOPCHOP v2: a web tool for the next generation of CRISPR genome engineering. Nucleic Acids Res. 44, W272–W276. https://doi.org/10.1093/nar/gkw398.
- Hwang, W.Y., Fu, Y., Reyon, D., Maeder, M.L., Tsai, S.Q., Sander, J.D., Peterson, R.T., Yeh, J.R.J., and Joung, J.K. (2013). Efficient genome editing in zebrafish using a CRISPR-Cas system. Nat. Biotechnol. 31, 227–229. https://doi.org/10.1038/nbt.2501.
- Ablain, J., Durand, E.M., Yang, S., Zhou, Y., and Zon, L.I. (2015). A CRISPR/Cas9 vector system for tissue-specific gene disruption in zebrafish. Dev. Cell 32, 756–764. https://doi.org/10.1016/j.devcel.2015.01.032.

- Meeker, N.D., Hutchinson, S.A., Ho, L., and Trede, N.S. (2007). Method for isolation of PCR-ready genomic DNA from zebrafish tissues. BioTechniques 43, 610–614. https://doi.org/10.2144/000112619.
- Choi, H.M.T., Schwarzkopf, M., Fornace, M.E., Acharya, A., Artavanis, G., Stegmaier, J., Cunha, A., and Pierce, N.A. (2018). Third-generation in situ hybridization chain reaction: multiplexed, quantitative, sensitive, versatile, robust. Development 145, dev165753. https://doi.org/10.1242/dev. 165753.
- Ravi, N., Gabeur, V., Hu, Y.-T., Hu, R., Ryali, C., Ma, T., Khedr, H., Rädle, R., Rolland, C., Gustafson, L., et al. (2024). SAM 2: Segment Anything in Images and Videos. Preprint at arXiv. https://doi.org/10.48550/arXiv. 2408.00714.
- Jia, B.Z., Qi, Y., Wong-Campos, J.D., Megason, S.G., and Cohen, A.E. (2023). A bioelectrical phase transition patterns the first vertebrate heart-beats. Nature 622, 149–155. https://doi.org/10.1038/s41586-023-06561-z.

Current Biology Report



STAR*METHODS

KEY RESOURCES TABLE

REAGENT or RESOURCE	SOURCE	IDENTIFIER
Antibodies		
Rabbit polyclonal anti-Piezo1	ThermoFisher	15939-1-AP; RRID: AB_2231460
Rabbit polyclonal anti-beta tubulin	Abcam	ab6046; RRID: AB_2210370
Peroxidase AffiniPure F(ab')₂ Fragment Goat Anti-Rabbit IgG (H+L)	Jackson ImmunoResearch Laboratories Inc.	111-036-045; RRID: AB_2337943
Chemicals, peptides, and recombinant proteins		
_ow-melt agarose	National Diagnostics	EC-204
MS-222 (tricaine)	Millipore Sigma	E10521
ubocurarine hydrochloride	Millipore Sigma	T2379
Ruthenium red	Millipore Sigma	557450
Streptomycin	Millipore Sigma	S6501
Gadolinium (III) chloride	Millipore Sigma	G7532
2-aminoethoxydiphenyl borate (2-APB)	Millipore Sigma	100065
D-GsMTx4	MedChemExpress	HY-P1410B
AlexaFluor594-Dextran 10000 MW	Life Technologies	D22913
Kainic acid	Millipore Sigma	K0250
Cas9	PNA Bio Inc.	CP01
Complete Protease Inhibitor Cocktail	Millipore Sigma	11697498001
RIPA Buffer	Millipore Sigma	R0278
Critical commercial assays		
nMESSAGE mMACHINE SP6 Transcription Kit	ThermoFisher	AM1340
nMESSAGE mMACHINE T7 ULTRA Transcription Kit	ThermoFisher	AM1345
Amersham ECL Prime Western Blotting Detection Reagent	Cytiva	RPN2232
Micro BCA Protein Assay Kit	ThermoFisher	23235
Platinum Hot Start PCR Master Mixes	ThermoFisher	13000012
Hybridization Chain Reaction v3.0 kit	Gene Tools	No longer sold
Experimental models: Organisms/strains		
g(kdrl:Gal4;myl7:eGFP)	Kim et al. ⁵⁷	ZDB-TGCONSTRCT-150504-3
g(UAS:GCaMP5G)	Fidelin et al. ⁵⁸	ZDB-TGCONSTRCT-150417-4
g(vglut2a:Gal4;UAS:GCaMP6s)	Satou et al. ²³ and Muto et al. ⁵⁹	ZDB-TGCONSTRCT-131127-1, ZDB-TGCONSTRCT-170615-2
g(kdrl:eGF)	Beis et al. ⁶⁰	ZDB-TGCONSTRCT-070117-47
Dligonucleotides		
notch3 HCR probe set	Integrated DNA Technologies (O'Brown et al. 61)	N/A
nnt3b Morpholino (5'-AACATCCTCA GTATCAGACATGATG-3')	GeneTools (Ferrante et al. ⁶²)	ZDB-MRPHLNO-110228-4
nnc2 Morpholino (5'-GTATATAGACA	GeneTools (This study)	N/A
oiezo1 sense photo-cleavable morpholino 5'-AGGAATGTGAAAPTTAGTGTCGCTC-3')	GeneTools (This study), no longer sold	N/A
piezo1 anti-sense morpholino (5'-GAGC GACACTTCCACTCACATTCCT-3')	GeneTools (This study)	N/A
CRISPR gRNAs (see Table S1)	This study	N/A
- ,	•	(Continued on next or

(Continued on next page)





Continued		
REAGENT or RESOURCE	SOURCE	IDENTIFIER
Genotyping primers for piezo1, pkd2, trpv4 (see Table S1)	Integrated DNA Technologies (this study)	N/A
Software and algorithms		
Custom software/code	This study	DOI: 10.5281/zenodo.17330879
Luminos	Itkis et al. ⁶³	https://www.luminosmicroscopy.com/
FIJI	NIH Image	https://imagej.nih.gov/ij/
Adobe Illustrator	Adobe, San Jose, CA	https://www.adobe.com/ products/illustrator.html

EXPERIMENTAL MODEL AND STUDY PARTICIPANT DETAILS

Zebrafish

Animal experiment protocols were approved by the Harvard University Institutional Animal Care and Use Committee. All wild-type (WT) and transgenic zebrafish (*Danio rerio*) were raised and bred on a 14/10-hour light/dark cycle at 28.5 °C following standard procedures. Experiments were performed between 2 and 7 days post fertilization. Zebrafish sex cannot be determined until 3 weeks post-fertilization, so experimental animals' sex was unknown. All sample sizes are reported in figure captions.

To obtain transgenic strains which express GCaMP5G in cytoplasm of vascular endothelial cells, the transgenic lines $Tg(kdrl:Gal4;myl7:eGFP)^{57}$ and $Tg(UAS:GCaMP5G)^{58}$ were crossed, and offspring were screened by fluorescence expression pattern for imaging experiments at desired stages. To obtain larvae expressing GCaMP6s in vascular endothelial cells and/or glutamatergic interneurons, Tg(kdrl:Gal4;myl7:eGFP) fish were crossed with Tg(vglut2a:Gal4;UAS:GCaMP6s) fish. 23,59 Tg(kdrl:eGFP) fish 60 (casper background) were crossed against AB fish to generate larvae with calcium-independent fluorescence in the endothelial cells.

METHOD DETAILS

Microscopy and imaging

All embryos and larvae were raised in E3 media (5 mM NaCl, 0.17 mM KCl, 0.33 mM CaCl₂, and 0.33 mM MgSO₄). Before imaging experiments, embryos and larvae were manually mounted in 2% low-melting-point agarose lateral-side down on glass-bottom petridishes (MatTek or CellVis) for inverted microscope imaging, or on an agarose trench for upright microscope imaging.

To document expression pattern and morphology, fish were imaged on a custom-built ultra-widefield microscope or a spinning disk confocal microscope (Nikon Eclipse Ti2, Yokogawa CSU-W1). Functional calcium imaging, mechanical force application, violet light stimulation, and electrical field stimulation experiments were conducted for fish at 2-7 days post fertilization (dpf) using a custom-built epifluorescence microscope at room temperature. Illumination was provided by a solid state 488 nm laser (Coherent Obis 1226419, 100 mW), or a 488 nm 300 mW LED (LED Engin) driven by a current driver (Thorlabs DC4100).

Imaging was performed using 2x (Olympus MVPLAPO 2 XC), 4x (Olympus Fluor, NA 0.24), or 10x (Olympus UPlanSApo, NA 0.40; XLPLN10XSVMP, NA 1.0) objectives. A quad-band emission filter (Semrock Di01-R405/488/561/635) separated fluorescence from excitation light. Fluorescence passed through a 510/50 bandpass emission filter (Chroma) and was captured by a scientific CMOS camera (Hamamatsu Orca Flash 4.0). Custom LabView (National Instruments) software controlled the microscope as previously described. 64,65

Blood flow imaging was performed through a 10x objective (Olympus XLPLN10XSVMP, NA 1.0) at 500 Hz (Hamamatsu Orca Flash 4.0) using a red LED (Thorlabs M625L4) and a 647 nm/40 nm bandpass filter). Blood cells were manually traced from frame to determine velocity. In pharmacological treatment experiments, intersegmental vessels immediately posterior to the swim bladder of 5 dpf larvae were selected for Ca²⁺ imaging.

Visual stimulation to evoke twitch responses

Violet light visual stimulus was performed through a 10x objective (Olympus XLPLN10XSVMP, NA 1.0) by aligning a 405 nm laser (Coherent Obis LX 1284371, 100mW) onto the eye of the fish. Laser power was set to 20-50 mW. 405 nm light was delivered for periods of 10 seconds every 60 seconds.

Mechanical compression of larvae

Larvae were lightly anesthetized with tricaine (\sim 120 mg/L) and embedded in 1.5% low-melt agarose (Aquapor) covering the inner well of a 35 mm glass bottom dish (CellVis). Excess agarose was removed using a 6 mm biopsy punch. Imaging was performed as described in "microscopy and imaging", using an Olympus UPlanSApo 10x NA 0.40 objective on an inverted microscope. After the start of an acquisition, a 10 g scale calibration weight (\sim 10 mm diameter) was placed on the agarose pad using tweezers to provide a mechanical compression force on the fish.

Current Biology Report



Electrical stimulation of fish motion

Electrical stimuli were used to evoke twitches (Figure 4) before we identified a visual stimulus protocol that reliably evoked twitches. A chlorided silver wire was inserted inside a 6 M Ω borosilicate glass pipette (VWR Inc.), filled with E3 media. The pipette was positioned near the fish head. A counter-electrode of chlorided silver was placed near the fish tail. Electrical stimulation was applied using a high-voltage amplifier (Krohn-hite 7600M) to amplify 100 μ s square pulse generated by the DAQ card (NI BNC-2090A) to 30-45 V. Electrical stimulation did not affect fish heart rate, and fish remained viable for several days after electrical stimulation.

Pharmacological treatments

In visual stimulus experiments, para-aminoblebbistatin dissolved in DMSO (final concentration 0.5%) was diluted to a final concentration of 50 μ M in E3 media, to inhibit fish muscle contraction. Fish mounted in agarose were soaked for >30 minutes at 28.5 °C prior to imaging. To block the neuro-muscular junction, tubocurarine hydrochloride pentahydrate (Sigma Aldrich T2379-100MG) at 2.2 mM was applied to fish for > 1 h at 28.5 °C prior to imaging.

In mechanical compression experiments, larvae were pre-incubated in 3 μ M ruthenium red (Sigma 557450), 1 mM streptomycin (Sigma S6501), or 100 μ M gadolinium (III) chloride (Sigma G7532) for 1 – 2 hours, and embedded in 1.5 % low melt agarose containing the same concentrations of drugs and 120 mg/L tricaine. 2-aminoethoxydiphenyl borate (2-APB, Sigma 100065) was applied similarly at 20 μ M but with the addition of 0.3% DMSO and only for 20 minutes before mounting. D-GsMTx4 (MedChemExpress HY-P1410B) suspended in physiological extracellular buffer was injected intracardially (2 nL total volume) at 360 femtomols, using AlexaFluor594-Dextran 10000MW (Life Technologies D22913) as a tracer to confirm delivery into the bloodstream.

In long-term motion inhibition experiments, the following treatments were applied. 120 mg/L tricaine was applied to the embryo water and water was exchanged daily. 1.25 ng kainic acid dissolved in physiological extracellular buffer was injected beneath the hindbrain to ablate motor activity via excitotoxicity. 66 D-GsMTx4 was injected as described above, but was repeated daily. *tnnt3b* morpholino 62 (translation blocking) at 6 ng and *tnnc2* morpholino (splice-blocking, newly designed sequence 5'-GTATATAGA-CAACTCACCGGCAAGC-3') at 2 ng were co-injected at the 1-cell stage (8 ng Gene Tools standard control morpholino was used as control).

CRISPR/Cas9 knockouts

Cas9 protein (CP01) was acquired from PNA Bio Inc. Sequences of all gene-specific sgRNAs were designed using http://chopchop.cbu.uib.no/.⁶⁷ The selected sgRNAs were synthesized following established protocols. ^{68,69} All Cas9 proteins and home-synthesized sgRNAs were purified, aliquoted and stored at -80 °C until use.

For knockout experiments, a mixture of selected sgRNAs (1 μ L of each sgRNA at 300 ng/ μ L), Cas9 protein (1.2 μ L at 2 mg/mL), and phenol red dye (0.3 μ L) were freshly prepared 30 minutes prior to injection. Zebrafish zygotes were injected at single-cell stage with 500 pL of mixture through the chorion. At 24-30 hpf, injected zygotes were inspected under a Leica stereomicroscope.

To identify knockout efficiency, genomic DNA of injected and control intact zygotes (10 embryos each group) at desired development stages were extracted using the HotSHOT method. The gene sequences and sgRNA target sites of interest were amplified by Platinum Taq PCR reaction (Life Technologies 13000012). The cleavage patterns were visualized by gel electrophoresis using 2% agarose gel, 1x TAE buffer (Fisher Scientific AM9869), 6x purple loading dye (NEB B7024S), and TriDye 100 bp DNA ladder (NEB N3271S). For sequence analysis of cleaved gene sites, the sgRNA target sites were cloned into pENTR/D-TOPO vector (Thermo Fisher K240020), and sent for Sanger sequencing (Genewiz, Inc.). The mutant sequences were identified by comparison to wild-type sequence from intact zygotes.

To knock out *piezo1* expression, we designed five sgRNAs that mutated the 5' untranslated region (5'-UTR) of the *piezo1* locus, and another five sgRNAs that mutated the start region of first exon, including start codon (Figure S7A). We confirmed this 351-base pair excision by gel electrophoresis (Figure S7B) and sequencing (Figure S7C) of CRISPR/Cas9 injected embryos. To knock out *pkd2* expression, we designed 2 groups of sgRNAs to target two regions in the first exon, separated by 340 base pairs (Figure S7A). We confirmed this 340-base pair excision by gel electrophoresis (Figure S7B) and sequencing (Figure S7C) of CRISPR/Cas9 injected embryos. The TRPV4 gene of zebrafish has relatively short Exon 1 and Exon 2, yielding limited sites for sgRNA binding. We thus designed 2 groups of sgRNAs to mutate 2 regions within its long Exon 3, separated by 560 base pairs (Figure S7A). We confirmed this 560-base pair excision by gel electrophoresis (Figure S7B) and sequencing (Figure S7C) of CRISPR/Cas9 injected embryos. All guide RNA sequences and genotyping primers are included in Table S1.

Morpholino/Photo-morpholino knockdown

All antisense morpholino oligonucleotides and sense photo-cleavable morpholino oligonucleotides were purchased from Gene Tools, LLC. The concentration of morpholino in solution was determined using a spectrophotometer with a 1 cm path length (Thermo Scientific NanoDrop 2000/2000c). The light-induced cleavage of photo-morpholino was verified by mass spectroscopy at Gene Tools, LLC. For the Piezo1 knockdown experiments by photo-morpholino, each embryo of Tg(kdrl:Gal4:UAS:GCaMP5G) or control wild-type (AB or PE) line at single-cell stage was injected with 1.16 nL of duplex, containing 2.5 ng of 1.016 mM piezo1 antisense morpholino oligonucleotides and 2.5 ng of 1.029 mM piezo1 sense photo-cleavable morpholino oligonucleotides. At 3 dpf, the injected and control embryos were exposed to 355 nm laser for 30 seconds to cleave the photo-sensitive antisense morpholino. At 5 dpf, functional calcium imaging of larvae was carried out on a custom-built epi-fluorescence microscope, followed by lysis treatment for western blotting analysis.





Western blot analysis

After calcium imaging measurements, all recorded and control fish were separately lysed in ice-cold RIPA lysis buffer (Sigma Aldrich R0278) complemented with 1:100 protease inhibitor (Sigma Aldrich 11697498001). To quantify and compare their Piezo1 expression, β-tubulin expression was used as loading control. Following incubation at 4 °C for 20 minutes, the lysed solution was centrifuged at 16,000 g for 1 hour at 4 °C, and supernatant was retained, followed by the protein concentration determination by microBCA protein assay at 562 nm (Thermo Fisher Scientific 23235). For single fish at 6 dpf, we generally get 100 uL of lysed solution at 0.5 mg/mL protein concentration. Each lysed solution was added with 95 °C 5x Laemmli buffer (2.5 mL of 1.25 M Tris at pH 6.8, 5 mL of 100% glycerol, 1g of electrophoresis grade SDS, 0.8 g of electrophoresis grade DTT, and 1 mL of 1% bromophenol blue) and sonicated briefly for 30 seconds. The protein solutions were then boiled at 37 °C for 10 minutes, followed by brief vortex for 30 seconds and spin down (14,600 rcf, Relative Centrifuge Force) at room temperature.

The protein solutions were loaded into NuPAGE Novex 3-8% Tris-Acetate gels (Thermo Fisher Scientific EA0375BOX) with \sim 40 μ g protein mass per lane and incubated in NuPAGE Tris-Acetate SDS running buffer (Thermo Fisher Scientific LA0041). Since Piezo1 protein has large molecular weight \sim 270 kDa, 42 a Spectra multicolor high range protein ladder (Thermo Fisher Scientific 26625) was chosen for reference. The electrophoresis was carried out for 20 minutes at 80 V followed by 1 hour at 120 V. Gels and 2 pieces of fresh pre-cut extra-thick blotting paper (Bio-rad 1703965) were rinsed in cold 4 °C NuPAGE transfer buffer (Thermo Fisher Scientific NP0006-1) for 2 minutes. Prior to blotting, an immune-blot PVDF membrane (Bio-rad 4569035) was activated in 100 % MeOH for 1 minute and rinsed in same 4 °C NuPAGE transfer buffer for 2 minutes. The transfer sandwich was assembled in the order: extra-thick blotting paper, activated PVDF membrane, gel, extra-thick blotting paper. Air bubbles trapped inside were squeezed out by a roller. A Bio-rad semi-dry and rapid blotting system was used to complete the transfer process at 2.5 A for 15 minutes.

Following transfer, the blotted membranes were inspected under light and rinsed in casein blocking buffer (Sigma Aldrich B6429) overnight at 4 °C. Piezo1 protein is a trimer, containing \sim 2,547 AA (\sim 900 kDa), and becomes dissociated into monomer under denaturing conditions. Membranes were split along 150 kDa mass line into 2 pieces, which contained the Piezo1 monomer (\sim 270-300 kDa)⁴² and β -tubulin (55 kDa; loading control), respectively. The split membranes were incubated with 10 mL of primary Piezo1 rabbit polyclonal antibody (1: 5000 in Casein blocking buffer, Fisher Scientific 15939-1-AP) and primary β -tubulin rabbit polyclonal antibody (1: 5000 in Casein blocking buffer, Abcam ab6046) at room temperature for 1 hour, followed by 5 rinses of 10 min each in TBST buffer at pH 7.62 (20 mM Tris, 150 mM NaCl, and 0.05% Tween 20). All rinsed membranes were incubated with peroxidase goat anti-rabbit IgG secondary antibody (1:2000 in Casein blocking buffer, Jackson Immuno Research Inc. 111-036-045) at room temperature for > 2 hours, followed by 5 rinses of 10 min each in same TBST buffer. The rinsed membranes were added with 1 mL of chemiluminescence solution mixed from GE Healthcare Amersham ECL Prime western blotting detection reagent (Fisher Scientific RPN2232) and imaged immediately by an Azure Biosystems C400 imager at room temperature. The intensity of protein bands were quantified with normalization by loading control, β -tubulin, and compared by ImageJ and Adobe Photoshop.

Fluorescence in situ hybridization (HCR-FISH)

Third-generation HCR-FISH was performed for *notch3* to mark vascular mural cells as previously described. ^{61,71} Briefly, larvae were fixed in 4% paraformaldehyde in PBS (pH 7.2) overnight and stored in methanol at -20 °C until staining. Larvae were rehydrated in a series of methanol/PBST (0.1% Tween) washes and then permeabilized with 30 μg/ml Proteinase K (Life Technologies EO0491) for 45 min at room temperature. Larvae were then refixed in freshly made 4% PFA for 20 min and treated with probe hybridization buffer (Molecular Instruments) at 37 °C. *notch3* probes ⁶¹ were added (4 nM) for 18 h rocking at 37 °C. The next day, larvae were washed with probe wash buffer (Molecular Instruments) at 37 °C and 5x SSCT (5x saline sodium citrate with 0.1% Tween 20) at room temperature. Excess liquid was removed and samples were immersed in amplification buffer (Molecular Instruments) at room temperature for 30 min prior to hairpin amplification, which occurred overnight rocking at room temperature at concentration of 15 pmol. Larvae were then washed in 5x SSCT and embedded in low-melt agarose (in PBS) for imaging.

QUANTIFICATION AND STATISTICAL ANALYSIS

Data analysis, statistics, and plotting were performed in MATLAB and Python (using Numpy, Scipy, and related libraries). Statistical details can be found in the figure legends. Statistical significance was defined by p < 0.05 with Benjamini-Hochberg multiple hypothesis correction. p-values are reported directly in figure legends.

In whole-fish recordings, body strain was determined by manually selecting a line along the body axis, generating a kymograph, and calculating the change in the mean distance between intersegmental vessels at each timepoint by spatial autocorrelation. For visual stimulus experiments where displacement was large relative to the field of view, relative motion was instead determined using the spatial Fourier transform of a strip of video along the animal body axis. The amount of low frequency signal in the power spectrum, or "blurring" beyond the time resolution of the recording, relative to that at rest was used as an indication of motion. Motion correction was performed using least-squares estimation of Euclidean transformation matrices between frames at a manually adjusted spacing

Current Biology Report



(MATLAB 'imregtform'). These transformation matrices were then linearly interpolated between frames. In experiments combining visual stimulus and pharmacology, vessel segmentation was performed using Segment Anything 2 (a deep learning model).⁷² In other experiments, vessel segmentation was performed manually, by drawing regions of interest (genetic knockout/knockdown experiments), or by tracing the intensity kymographs of lines drawn perpendicularly to intersegmental vessels (whole-fish and weight press experiments). Analysis of Ca²⁺ imaging data was then performed as previously described.⁷³

Analysis code is on Zenodo: DOI: 10.5281/zenodo.17330879.